

## Size-Dependent Electrochemical Oxidation of Silver Nanoparticles

Olga S. Ivanova and Francis P. Zamborini\*

Department of Chemistry, University of Louisville, Louisville, Kentucky 40292

Received October 14, 2009; E-mail: f.zamborini@louisville.edu

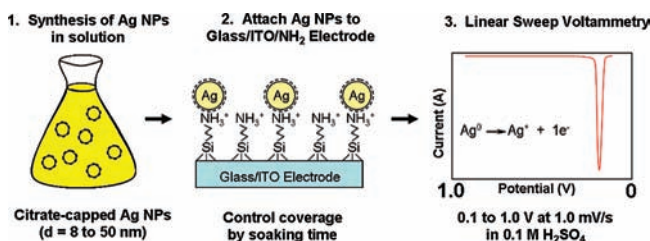
Understanding the thermodynamics and kinetics of the electrochemical oxidation of metal nanostructures is extremely important considering their numerous potential applications in electrooptics, sensing, catalysis, and nanoelectronics and the importance of metallic corrosion. Stability against oxidation is critical for metal nanostructures to retain their useful properties. There has been some theoretical work<sup>1–6</sup> and scanning tunneling microscopy (STM) observations<sup>7,8</sup> of metal nanoparticles undergoing oxidation, but very few direct electrochemical or microscopic measurements<sup>5,6</sup> as a function of size and shape. Here we describe the voltammetry of Ag nanoparticle (Ag NP) oxidation as a function of size.

There are two main reasons to expect size-dependent electrochemical oxidation of metal nanoparticles. First, theoretical and experimental studies showed that the standard redox potential of metal nanoparticles decreases with decreasing size. For example, Henglein predicted large negative shifts in the redox potential for small Ag<sub>n</sub> clusters (*n* = 1 to 15) as the number of atoms in the cluster decreases.<sup>2</sup> Plieth similarly predicted a negative shift in the redox potential proportional to (1/radius) for small nanoparticles relative to the bulk metal based on the difference in surface free energy between bulk metal and the same number of atoms dispersed into smaller NPs.<sup>1</sup> Experimentally, Brus and co-workers showed that large Ag NPs grow at the expense of small NPs on a conductive surface (Ostwald ripening) due to the predicted negative shift in oxidation potential for smaller sizes.<sup>9</sup>

The work of Compton and co-workers offers a second explanation for size-dependent electrochemical oxidation of metal nanoparticles. Their work addresses the oxidation (stripping) of an array of metal nanoparticles attached to a conductive electrode surface.<sup>4–6</sup> The different electrochemical behavior is based on the size-dependent diffusion profiles of the metal ions that emanate from the oxidizing array of nanoparticles. Under the assumption that *E*<sup>0</sup> does *not* shift with particle size, theory predicts that in electrochemical reversible systems the peak potential (*E*<sub>p</sub>) depends on the metal coverage, but not the NP radius under conditions where the diffusion layers of the nanoparticles overlap (planar diffusion) and vice versa when they do not overlap.<sup>5</sup> Under conditions of planar diffusion, the oxidation of Ag NPs (diameter = 25 to 100 nm) on a basal-plane pyrolytic graphite electrode did not exhibit a size-dependent *E*<sub>p</sub> experimentally.<sup>5</sup> In irreversible systems, theory predicts that *E*<sub>p</sub> is independent of metal coverage but shifts negative as the NP radius decreases.<sup>6</sup>

Microscopy studies have shown that tiny clusters of Cu on Au<sup>10</sup> and Ag on graphite<sup>11</sup> (<1.0 nm) exhibit greater stability against electrochemical oxidation (+200 to +500 mV) compared to the bulk metal, contrasting the predictions of Plieth<sup>1</sup> and Henglein.<sup>2</sup> These results raise interesting questions about the electronic, structural, and chemical effects of the electrode–metal interaction on metal nanoparticle oxidation potential and kinetics.<sup>7,11,12</sup> These studies lacked direct electrochemical measurements. Clearly there

**Scheme 1.** Method for Measuring the Oxidation Potential of Ag Nanoparticles As a Function of Size



is a need to directly characterize the oxidation of metal nanoparticles electrochemically to better understand the effect of size and electrode material.

Scheme 1 illustrates our experimental procedure. In step 1, we synthesized different sized citrate-capped Ag NPs, ranging in diameter from approximately 8 to 50 nm, by a seed-mediated growth procedure.<sup>13</sup> This involved the synthesis of Ag NP “seeds” first by the reduction of AgNO<sub>3</sub> with NaBH<sub>4</sub> in water in the presence of trisodium citrate. We then synthesized larger sizes by growing the Ag NP “seeds” into larger NPs by heating a solution of Ag NP “seeds”, AgNO<sub>3</sub>, and trisodium citrate. The final diameter of the grown Ag NPs increased with increasing AgNO<sub>3</sub> (Ag<sup>+</sup>)/Ag seed mole ratio during the synthesis. In step 2, we immersed an amine-functionalized indium tin oxide (ITO) coated glass electrode (Glass/ITO/NH<sub>2</sub>) into a solution of the Ag NPs, which leads to electrostatic attachment. The coverage depended on the immersion time. In step 3, we performed linear sweep voltammetry (LSV) on the Glass/ITO/NH<sub>3</sub><sup>+</sup>/Ag NP electrode to directly measure *E*<sub>p</sub> for Ag oxidation. The full details of the three steps are in the Supporting Information (SI). The important features are (1) Ag NP size control, (2) attachment of Ag NPs through an organic linker to remove the effect of direct interactions between the Ag NPs and Glass/ITO on the oxidation, and (3) control of Ag NP coverage.

We characterized the different Ag NPs in solution by optical methods (Figures S1 and S2) and by atomic force microscopy (AFM) and scanning electron microscopy (SEM) after electrostatic attachment to Si/SiO<sub>x</sub>/NH<sub>2</sub> and Glass/ITO/NH<sub>2</sub> surfaces, respectively (Figures S3 and S4). Figure 1 shows typical SEM images of 4 different samples. Frame A shows an SEM image of Ag NP “seeds”, which are 8–12 nm in diameter. Frames B–D show Ag NPs synthesized with Ag<sup>+</sup>/Ag seed ratios of 10, 40, and 100 with average diameters of 26.6, 37.9, and 45.5 nm, respectively. The Ag NPs were fairly well-spaced and isolated on the surface (very few aggregates).

We obtained linear sweep voltammograms (LSVs) from 0.1 to 1.0 V in 0.1 M H<sub>2</sub>SO<sub>4</sub> at 1.0 mV/s of Glass/ITO/NH<sub>2</sub> electrodes coated with Ag NPs of different sizes (see Figure S5 of SI for all LSVs). Figure 2 shows LSVs in the range 0.20 to 0.45 V for electrodes coated with seed, ratio 10, ratio 40, and ratio 100 Ag

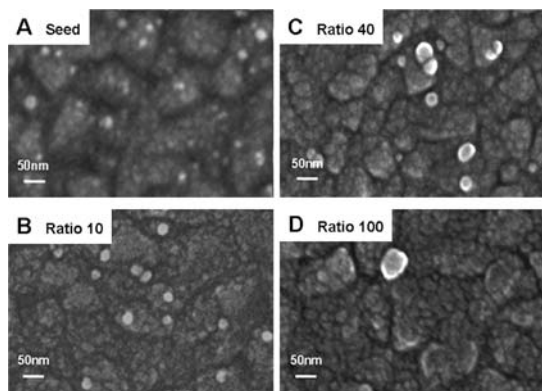


**Figure 1.** SEM images of Glass/ITO/NH<sub>2</sub> electrodes coated with (A) Ag seed NPs and Ag NPs synthesized by seed-mediated growth using Ag<sup>+</sup>/Ag seed ratios of (B) 10, (C) 40, and (D) 100.

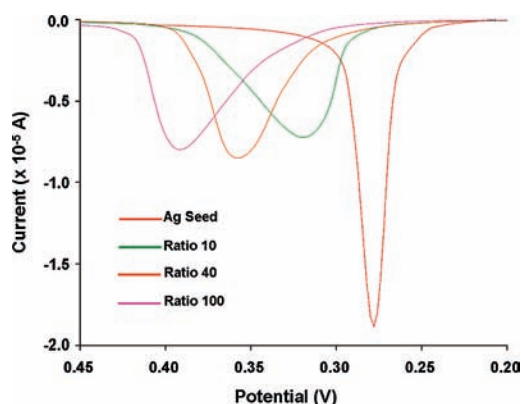


**Figure 2.** Linear sweep voltammograms (LSVs) obtained in 0.1 M H<sub>2</sub>SO<sub>4</sub> electrolyte at 1.0 mV/s of 1.4 cm<sup>2</sup> Glass/ITO/NH<sub>2</sub> electrodes coated with Ag seed NPs and larger Ag NPs synthesized by seed-mediated growth using Ag<sup>+</sup>/Ag seed ratios of 10, 40, and 100.

NPs with corresponding  $E_p$  values of 278, 320, 358, and 391 mV, respectively. The negative anodic current corresponds to the reaction of  $\text{Ag}^0 \rightarrow \text{Ag}^+ + 1e^-$ .  $E_p$  shifts positive with increasing Ag<sup>+</sup>/Ag seed ratio (or increasing size). We also observed experimentally that for a constant NP size,  $E_p$  was directly proportional to  $\ln(\text{Ag coverage})$  (see Figure S6 and Table S2, SI), which is expected for reversible Ag oxidation kinetics.<sup>5</sup> To rule out the effect of coverage, we kept the total coverage of Ag on the electrode surface constant within  $(3-5) \times 10^{-4}$  coulomb (C). The coverage in Figure 2 for seed, ratio 10, ratio 40, and ratio 100 Ag NPs was  $(4.6, 4.4, 4.5, \text{ and } 4.6) \times 10^{-4}$  C, respectively. We also observed that  $E_p$  shifts positive with increasing scan rate (see Figures S7, S8 and Table S3 of SI). Previous literature predicts that  $E_p$  is proportional to  $\ln(\text{scan rate})$ , which is in good agreement with our results.<sup>5</sup> We chose a slow scan rate of 1 mV/s to ensure electrochemical reversibility and conditions of planar diffusion (overlapping diffusion profiles). At 1 mV/s, the diffusion layer thickness ( $\delta$ ) is  $\sim 0.04$  cm  $[2(Dt)^{1/2}]$  over the  $\sim 45$  s time that it takes to oxidize the Ag (peak width 30–60 mV). The  $\delta$  is much larger than the average calculated Ag nanoparticle spacing of 50 nm for seed and 370 nm for ratio 100 Ag NPs, ensuring planar diffusion.

Table 1 shows the average diameter measured by AFM and SEM for the seed and different Ag<sup>+</sup>/Ag seed ratio Ag NPs along with average  $E_p$ , full width at half-maximum, and charge under the peak determined from the LSVs (at least 5 samples). The Ag NP diameter is in good agreement with the theoretical values at different ratios of Ag<sup>+</sup>/Ag seed based on the equation,  $d_p = d_{p0} (1 + n_+/n_s)^{1/3}$ , where  $d_p$  is the final diameter of the NP,  $d_{p0}$

**Table 1.** Statistical Size and Electrochemical Data for Glass/ITO/NH<sub>3</sub><sup>+</sup>/Ag NP Electrodes

Synthesis Ratio ( $n_+/n_s$ )	Diameter AFM (nm)	Diameter SEM (nm)	Theoretical diameter (nm)	Peak Potential $E_p$ (mV)	Full width at half max (mV)	Charge under the peak ( $\times 10^{-4}$ C)
0:0 (seed)	8.5 ( $\pm 3.3$ )	12.3 ( $\pm 3.5$ )	8.5	275 ( $\pm 25$ )	33 ( $\pm 10$ )	4.3 ( $\pm 1.7$ )
5:1	16.7 ( $\pm 6.9$ )	16.8 ( $\pm 5.4$ )	15.5	291 ( $\pm 11$ )	33 ( $\pm 13$ )	3.5 ( $\pm 0.9$ )
10:1	21.4 ( $\pm 6.3$ )	20.5 ( $\pm 4.3$ )	18.9	318 ( $\pm 6$ )	48 ( $\pm 11$ )	3.9 ( $\pm 0.5$ )
20:1	25.0 ( $\pm 6.5$ )	26.6 ( $\pm 5.1$ )	23.6	340 ( $\pm 4$ )	55 ( $\pm 8$ )	3.0 ( $\pm 0.2$ )
40:1	30.9 ( $\pm 8.9$ )	27.9 ( $\pm 8.7$ )	29.5	354 ( $\pm 7$ )	54 ( $\pm 15$ )	3.8 ( $\pm 1.0$ )
60:1	35.1 ( $\pm 12.3$ )	37.9 ( $\pm 11.0$ )	33.6	371 ( $\pm 10$ )	66 ( $\pm 19$ )	4.1 ( $\pm 0.8$ )
100:1	42.9 ( $\pm 13.2$ )	45.5 ( $\pm 15.1$ )	39.8	382 ( $\pm 9$ )	65 ( $\pm 20$ )	3.3 ( $\pm 0.7$ )

is the diameter of the Ag seed, and  $n_+/n_s$  is the Ag<sup>+</sup>/Ag seed mole ratio used in the synthesis.<sup>13</sup> The average  $E_p$  values shift positive with increasing Ag NP diameter and are all statistically different from one another except for the ratio 60 and 100 Ag NPs.  $E_p$  shifts  $\sim 107$  mV from the smallest seed particles to the largest ratio 100 Ag NPs.

Under the conditions of our experiment (reversible system, constant coverage, planar diffusion), previous theory based on diffusion alone predicts that  $E_p$  should *not* shift as a function of size.<sup>5</sup> For this reason, we believe the observed negative shift in  $E_p$  with size is *not* due to diffusion, but rather due to a negative shift in the standard redox potential ( $E^0$ ) as the size decreases as predicted by Plieth<sup>1</sup> and Henglein<sup>2</sup> and shown qualitatively by Brus.<sup>9</sup> This is the first direct measurement of this phenomenon by voltammetry. The graph in Figure 3 plots the difference between  $E_{p,\text{AgNP}}$  and  $E_{p,\text{BulkAg}}$  ( $\Delta E_p$ ) as a function of Ag NP radius (based on the AFM measurement) as compared to the prediction by Plieth.<sup>1</sup> We used  $E_p$  of the ratio 100 Ag NPs as  $E_{p,\text{BulkAg}}$  (382 mV). Our experimental  $\Delta E_p$  is larger than the theoretical prediction for all NP sizes except the two largest sizes, and they do not follow the theoretical trend, other than the general negative shift in potential with decreasing radius. The reasons for the discrepancy are not clear at this time. Clearly more work is needed to explain the data theoretically. Note that we used the surface stress ( $\gamma$ ) of Ag in vacuum for the theoretical plot.<sup>1</sup> The actual value for  $\gamma$  would be different in electrolyte solution due to adsorbate-induced stress, and it also depends on the electrode potential,<sup>14</sup> which would affect the theoretical values of  $\Delta E_p$ . Compton and co-workers previously showed no change in  $E_p$  for Ag NPs with diameters ranging from 25 to 100 nm.<sup>5</sup> Our results show an  $\sim 40$  mV shift for 25 nm diameter Ag NPs versus bulk Ag and no significant difference in  $E_p$  above 35 nm diameter NPs. The difference at 25 nm may be due to the aggregated state of the Ag NPs in the Compton work.<sup>5</sup>

Figure 4 shows three theoretical LSVs for the oxidation of  $\sim 5 \times 10^{-4}$  C of Ag from the electrode surface along with experimental

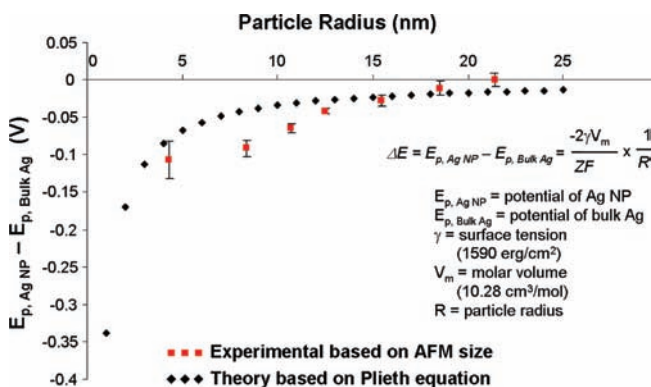


**Figure 3.** Experimentally measured shift in potential (■) for Ag NPs versus bulk Ag as a function of NP radius as compared to theory (◆).

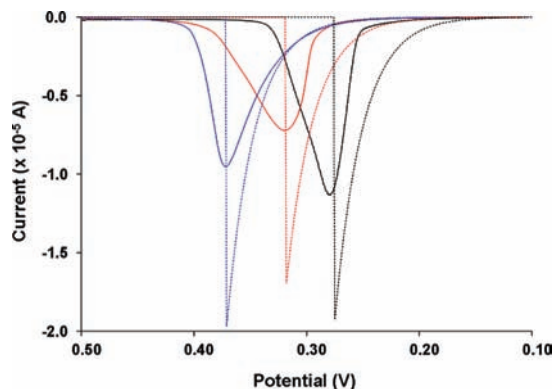


**Figure 4.** Theoretical LSVs (dotted lines) based on  $E^0$  values of 624 mV (blue), 575 mV (red), and 523 mV (black). Experimental LSVs (solid lines) for ratio 60 (blue), ratio 10 (red), and seed (black) Ag NPs. The coverages of the theoretical plots match the coverages of the experimental plots in the figure.

data. We used the following equation to determine the moles of Ag oxidized for each second when scanning from 0.1 to 1.0 V at 1.0 mV/s.

$$\text{mol Ag oxidized} = (C_{\text{Ag}^+(\alpha=0)}/2) \cdot \delta \cdot A \quad (1)$$

where  $C_{\text{Ag}^+(\alpha=0)}$  is the concentration of  $\text{Ag}^+$  at the electrode surface in  $\text{mol}/\text{cm}^3$  as determined by the Nernst equation,  $E = E^0 - 0.0592 \log(1/[\text{Ag}^+])$ ,  $\delta$  is the diffusion layer thickness [ $2(Dt)^{1/2}$ ], and  $A$  is the area of the working electrode ( $1.4 \text{ cm}^2$ ). This equation assumes a linear concentration profile from the electrode surface to the bulk solution where the concentration of Ag is 0. We converted the mol Ag oxidized at each second into coulombs to determine the current at each  $E$ . Once the total mol Ag oxidized exceeded the coverage of Ag, we decreased the current to 0, giving the sharp current drop off (Supporting Information provides more details). Figure 4 shows the theoretical LSVs using three different values of  $E^0$  to match the  $E_p$  of the experimental data at their specific coverages ( $(4-5) \times 10^{-5} \text{ C}$ ). The theory predicts that when  $E^0 = 623 \text{ mV}$ , the Ag NPs fully oxidize by 371 mV. This agrees well with the experimental  $E_p$  for ratio 60 Ag NPs. Theoretical  $E^0$  values of 575 and 523 mV fit the  $E_p$  for ratio 10 and Ag seed NPs, where the Ag fully oxidized by 318 and 275 mV, respectively. The standard redox potential for Ag/Ag<sup>+</sup> is 0.799 V vs NHE. We found our Ag/AgCl reference electrode was  $\sim 0.172 \text{ V}$  vs NHE based on a cyclic voltammogram of  $\text{Fe}(\text{CN})_6^{3-/4-}$ , giving a bulk  $E^0$  value of 0.627 V for Ag/Ag<sup>+</sup>. This value agrees well with the  $E^0$  of 0.623 V that best fits the ratio 60 Ag NP LSV. Ratio 60 and 100 Ag NPs ( $d = 35-45 \text{ nm}$ ) were not statistically different; both behave electrochemically as bulk Ag. The analysis is

consistent with our conclusion that the smaller Ag NPs exhibit a lower  $E_p$  value due to a negative shift in  $E^0$  for the Ag/Ag<sup>+</sup> redox couple. While this simple theory explains  $E_p$  fairly well, it does not predict the peak shape of the experimental plots. They do not drop off sharply. We do not fully understand the reason, but some possibilities could be the Ag NP size distribution, assumption of a linear concentration gradient, nonuniform attachment of Ag NPs to the surface, Ag aggregates on the surface, and the possible presence of the back reaction of Ag deposition due to electrochemical Ostwald ripening.<sup>9</sup>

In summary, we described the direct voltammetric measurement of  $E_p$  for Ag oxidation as a function of Ag NP size. Under our experimental conditions of planar diffusion, constant Ag coverage, and electrochemical reversibility, previous theory based on diffusion only predicts a constant  $E_p$  with size.<sup>5</sup> This fact and our theoretical LSVs suggest that the experimental shift in  $E_p$  is due to a size-dependent change in  $E^0$  for the Ag/Ag<sup>+</sup> redox couple. We also performed constant potential (Figure S9) and stirring (Figure S10) experiments suggesting that diffusion is not responsible for the change in  $E_p$  with size.

**Acknowledgment.** We gratefully acknowledge the National Science Foundation (CHE-0848883) for financial support of this research. We acknowledge K. J. Stevenson for helpful discussions. Olga Ivanova acknowledges Grzegorz Slawinski for assistance with SEM imaging.

**Supporting Information Available:** Experimental details, optical characterization, AFM/SEM images, plots of the effect of coverage and scan rate on  $E_p$ , theoretical calculations of  $E_p$ , and results of potential step and stirring experiments. This material is free of charge via the Internet at <http://pubs.acs.org>.

## References

- (1) Plieth, W. J. *J. Phys. Chem.* **1982**, *86*, 3166.
- (2) Henglein, A. *J. Phys. Chem.* **1993**, *97*, 5457–5471.
- (3) Grafov, B. M.; Paasch, G.; Plieth, W. J. *Electrochim. Acta* **2003**, *48*, 581–587.
- (4) Ward Jones, S. E.; Chevallier, F. G.; Paddon, C. A.; Compton, R. G. *Anal. Chem.* **2007**, *79*, 4110–4119.
- (5) Ward Jones, S. E.; Campbell, F. W.; Baron, R.; Xiao, L.; Compton, R. G. *J. Phys. Chem. C* **2008**, *112*, 17820–17827.
- (6) Ward Jones, S. E.; Toghill, K. E.; Zheng, S. H.; Morin, S.; Compton, R. G. *J. Phys. Chem. C* **2009**, *113*, 2846–2854.
- (7) Kolb, D. M.; Englemann, G. E.; Ziegler, J. C. *Angew. Chem., Int. Ed.* **2000**, *39*, 1123–1125.
- (8) Meier, J.; Kleine, H.; Stimming, U. *Surf. Sci.* **2005**, *597*, 127–132.
- (9) Redmond, P. L.; Hallock, A. J.; Brus, L. E. *Nano Lett.* **2005**, *5*, 131–135.
- (10) Kolb, D. M.; Simeone, F. C. *Electrochim. Acta* **2005**, *50*, 2989–2996.
- (11) Ng, K. H.; Liu, H.; Penner, R. M. *Langmuir* **2000**, *16*, 4016–4023.
- (12) Meier, J.; Friederich, K. A.; Stimming, U. *Faraday Discuss* **2002**, *121*, 365–372.
- (13) Pyatenko, A.; Yamaguchi, M.; Suzuki, M. *J. Phys. Chem. C* **2007**, *111*, 7910–7917.
- (14) Haiss, W. *Rep. Prog. Phys.* **2001**, *64*, 591–648.

JA908780G